Cis-Regulatory Editing of Peptide Signaling Rewires Plant Root Architecture

Authors

Jin C.-Y. Liao[1], Anne-Maarit Bågman[2,3,4], Angie J. Liu[1], Yejin Shim[1], Siobhán M. Brady[2,3,4] and Pamela C. Ronald[1,3,5,6]

Affiliations

[1]Department of Plant Pathology, University of California, Davis, CA, USA

[2]Department of Plant Biology, University of California, Davis, CA, USA

[3]Genome Center, University of California, Davis, CA, USA

[4]Howard Hughes Medical Institute (HHMI)

[5]Innovative Genomics Institute, University of California, Berkeley, CA, USA

[6]Joint Bioenergy Institute, Emeryville, CA, USA

Abstract

Precise *cis*-regulatory control of gene expression is essential for plant growth. In *Arabidopsis thaliana*, PLANT PEPTIDE CONTAINING SULFATED TYROSINE (PSY) peptides and their receptors (PSYRs) mediate growth-stress trade-offs, yet the transcriptional regulation of these genes remains poorly understood. Here, we mapped transcription factor (TF)-promoter interactions for nine *PSY* and three *PSYR* genes by combining high-throughput enhanced yeast one-hybrid screening with DNA Affinity Purification sequencing (DAP-seq) data, uncovering 1,207 interactions that reveal both shared and gene-specific regulatory relationships. Functional analysis of 25 TF mutants identified 12 regulators that significantly influence shoot and root growth, most acting as repressors. Of these, CYTOKININ RESPONSE FACTOR 10 (CRF10) emerged as a strong growth inhibitor. We identified a CRF10-binding motif in the PSYR3 promoter using DAP-seq data and validated it using eY1H. Guided by these insights, we used CRISPR/Cas9-mediated promoter editing to delete a small region encompassing or flanking a functional TF-binding site (TFBS). Removal of this motif, or of its surrounding region, reduced *PSYR3* expression and enhanced root growth, yielding variants that retained root length comparable to the *crf10* mutant. Together, our results define the global TF-promoter interaction network of the *PSYR/PSY* pathway and identify CRF10 as a key transcriptional regulator of *PSYR3*-mediated signaling. More broadly, our work demonstrates that targeting *cis*-regulatory regions can modulate gene expression and associated growth traits, suggesting a TFBS-focused strategy to influence plant growth patterns.

Introduction

Plants continuously face the fundamental challenge of balancing growth and defense, two competing physiological priorities essential for survival and reproduction. Growth maximizes biomass accumulation and competitive ability, while defense mechanisms protect against pathogens and herbivores. This trade-off is tightly regulated by complex signaling networks that integrate environmental cues with internal developmental programs. Small, secreted peptides have emerged as pivotal regulators in this process. The PLANT PEPTIDE CONTAINING SULFATED TYROSINE (PSY) family and their receptors (PSYRs) form a conserved signaling module in *Arabidopsis thaliana* that modulates cell expansion, root development, and various physiological responses[1–5]. PSY peptides promote growth by stimulating cell elongation and division while interfacing with defense pathways to fine-tune resource allocation. Despite their importance, the transcriptional mechanisms controlling *PSYR* and *PSY* gene expression remain poorly defined, limiting insight into how peptide signaling adapts dynamically to environmental and developmental cues. *Cis*-regulatory elements in gene promoters serve as binding platforms for transcription factors (TFs) that orchestrate gene expression spatially and temporally, but integrating high-throughput TF-promoter interaction data into functional regulatory modules remains challenging. Precise manipulation of such *cis*-elements for trait engineering is further complicated by redundancy and incomplete functional annotation.

CRISPR/Cas-mediated promoter and *cis*-regulatory element (CRE) editing provides powerful tools to fine-tune gene expression and optimize crop traits. Approaches include multiplexed promoter targeting, CRE disruption or deletion, and promoter insertion or swapping[6]. Multiplexed CRISPR/Cas tiling screens in tomato, maize, and rice have demonstrated the potential of systematic CRE editing, although large-scale identification of functional elements remains limited[7–9]. Targeted CRE disruption has enhanced stress responses and disease resistance. In rice, editing the GT-1 element ('GAAAAA') in the *Oryza sativa RAV2* (*OsRAV2*) promoter modulated salt tolerance[10], while deletion of a TALe (Transcription Activator-Like effector)-binding element in the *SWEET11*, a sugar transporter gene, promoter improved bacterial blight resistance without affecting fertility[11–13]. Similarly, mutations in barley's *Hordeum vulgare* purple acid phosphatase a (*HvPAPhy_a*) promoter reduced phytase activity[14], and disruption of Lateral Organ Boundaries 1 (LOB1) promoter elements in citrus conferred canker resistance[15–17]. CRE editing in introns or downstream regions further expands versatility, as shown by gain-of-function *Solanum lycopersicum* WUSCHEL (*SlWUS*) alleles in tomato[7,18]. Beyond plants, CRISPR-mediated disruption of transcription factor binding sites has been demonstrated in human cells and preclinical models[19]. In crops, understanding transcriptional networks that regulate growth-defense trade-offs, where activating defense often limits growth, will be critical for engineering resilient plants with optimized productivity. Promoter editing research has produced promising examples; however, tiling-deletion-based screens remain labor- and time-intensive, as they require analysis of numerous edited variants. Moreover, no gene regulatory network (GRN)-guided approach currently allows for precise, minimal modifications with predictive insight into the functional consequences of promoter elements, limiting the scalability of promoter editing.

Here, we integrated high-throughput enhanced yeast one-hybrid (eY1H) screening of nine *PSY* and three *PSYR* promoters with DAP-seq data to generate a comprehensive TF-promoter interaction network comprising over 1,200 interactions. Functional validation of selected TFs through loss-of-function mutant alleles and overexpression lines identified regulators modulating *PSYR/PSY* expression and growth phenotypes. Informed by this network, we implemented a CRISPR/Cas9-based promoter editing strategy to precisely delete selected transcription factor binding sites, enabling targeted modulation of *PSYR/PSY* expression. This work establishes a framework for mapping and manipulating transcriptional control of peptide signaling pathways, demonstrating how promoter editing can precisely optimize plant growth traits.

Results

Mapping the putative *PSYR*/*PSY* transcriptional regulatory network

To investigate transcriptional regulation underlying PSY peptide signaling, we performed enhanced yeast one-hybrid (eY1H) assays on three *PSYR* and nine *PSY* promoters using a curated *Arabidopsis* transcription factor (TF) consisting of 2,000 TFs[20]. Publicly available DAP-seq datasets[21] describe 1,207 TF-promoter interactions with ~500 TFs assessed. When integrated, these interactions revealed both shared and gene-specific regulatory relationships across the *PSYR*/*PSY* family, forming a comprehensive predictive transcriptional map controlling PSY and peptide transcription (Fig. 1 and Dataset S1). Network analysis further uncovered clusters of TFs potentially coordinating growth and defense responses, and several central hubs emerged as candidate regulators for functional validation. eY1H assays identify promoter-TF interactions in a chromatinized context in yeast, which can reveal potential regulatory relationships but may include false positives and negatives. Published studies have shown that a subset of eY1H-identified interactions is supported by *in planta* validation, such as ChIP or genetic analysis[22,23]. In contrast, DAP-seq profiles interactions between individual TFs and DNA sequences *in vitro*, providing high-resolution information on potential binding sites but not direct evidence of *in vivo* occupancy[21]. Integration of both datasets revealed limited overlap between the two datasets. Specifically, three TFs were identified to interact with the *PSYR1* promoter, eight for *PSYR2*, six for *PSYR3*, sixteen for *PSY1*, four for *PSY2*, two for *PSY3*, seven for *PSY4*, one for *PSY5-8*, and three for *PSY9* (Fig. S1 and Dataset S2). Together, these shared interactions highlight a small but robust set of candidate regulators supported by both approaches[24].

To investigate how these regulatory interactions are reflected *in planta*, we examined gene expression patterns across tissues and cell types. Analyses of publicly available RNA-seq datasets[25] defined the expression profiles of *PSYR* and *PSY* genes throughout Arabidopsis organs. All three *PSYR*s were broadly expressed, with *PSYR1* enriched in shoots and *PSYR3* in roots (Fig. S2). Among the peptides, *PSY1* was the most abundant and widely expressed, whereas *PSY7* showed minimal expression. *PSY4* was predominantly localized to roots, and *PSY9* was mainly expressed in seeds (Fig. S2). Single-cell data from the Plant sc-Atlas[26] further revealed cell-type specificity. *PSY3* and *PSY4* co-localized in root cell types, suggesting overlapping functions, while *PSY6* and *PSY8* displayed distinct but complementary root-specific patterns (Fig. S3). Together,

these findings highlight potential links between spatial regulation, receptor-ligand interplay, and root system architecture (RSA).

Network-guided selection and screening of TFs for promoter editing

To systematically prioritize transcription factors (TFs) for functional analysis, we combined whole-promoter interaction assays (eY1H) with DAP-seq data, identifying 40 high-confidence candidates. From these, 12 TFs with available homozygous mutant lines and an additional 10 TFs detected only by DAP-seq (represented by 13 independent homozygous alleles) were selected for phenotypic analysis (Dataset S2, S3, Table S2). Using these prioritized TFs, we then mapped their respective transcription factor binding sites (TFBS) across all three *PSYR* and nine *PSY* promoters to identify precise promoter regions for targeted editing. We focused on root system architecture (RSA) as a readout, given its responsiveness to genetic and environmental cues and the availability of high-throughput phenotyping tools. We then developed a workflow integrating TFBS mapping with functional assays to pinpoint regulatory regions suitable for CRISPR-based promoter editing (Fig. 2a). Although a root-specific DAP-seq dataset would be ideal, it is not currently available, underscoring the importance of combining multiple data sources for candidate prioritization.

While *PSY1* overexpression and the *psyr1,2,3* triple mutant has been reported to alter primary root length[1–3,27], other RSA phenotypes in these lines, as well as in single PSY or PSYR mutants, remain unknown. Given the root cell type expression patterns of *PSYR*/*PSY* genes, we focused on phenotypic analysis of mutants for the 12 TFs identified by both eY1H and DAP-seq. Knockouts were first validated by PCR genotyping and qRT-PCR (Fig. S5). Single mutant alleles of ten TF mutants (*crf10*, *tga2 tga5*, *wrky8-1*, *myb77-2*, *myb73-1*, *hb34*, *myb70-2*, *at3g42860*, *abi5-10*, *wrky14*) displayed increased primary root length, while two mutants (*rap2.11*, *atrav1.1*) showed no change (Fig. 2b-d). In addition to these 12 TFs, we also analyzed DAP-seq-only candidates for phenotypic effects, as homozygous mutant lines were available and they could reveal additional regulators of root growth not detected by eY1H. Among the DAP-seq-only TFs, six alleles of four TFs (*wrky22-1, wrky22-2, wrky22-3, anac087-2, erf11, aif*) displayed increased root length, one allele (*ein3-1*) showed decreased root length, and seven alleles (*hca2, pear2, myb3r4-3, tga10, ntl4-1, erf4-1, ntl8-1*) exhibited no change (Fig. S6). Many of these alleles had been studied previously, but root phenotypes were largely unreported or poorly described, with *myb70-2* as the only clearly documented case[28], showing a longer primary root consistent with our observations. Overall, 26 mutants of 24 TFs exhibited significant changes in root growth compared with wild-type plants, 16 of which displayed increased biomass and enhanced RSA, suggesting that multiple TFs negatively regulate growth to fine-tune developmental outcomes (Data S3). We tested the less-characterized candidate CRF10 and found that overexpression caused stunted growth, whereas the *crf10* knockout displayed enhanced growth compared with wild type (Fig. 2 b-d and Fig. S7). Collectively, these results demonstrate that the identified TFs contribute to root growth regulation, highlighting the potential of promoter-targeted approaches to modulate RSA phenotypes.

Organ-specific transcriptional rewiring in TF knockout lines

To assess whether candidate TFs act as activators or repressors of *PSYR*/*PSY* transcription and whether their regulation is organ-specific, we measured transcript levels in shoots and roots of selected TF knockout lines using quantitative RT-PCR (qRT-PCR) (Fig. 3). The same homozygous knockout lines that were genotyped and phenotypically validated in Fig. 2c were used for these expression assays, ensuring that transcriptional differences could be directly linked to previously observed RSA phenotypes. We focused on the three *PSYR* and three *PSY* (*PSY1*, *PSY2*, *PSY4*) promoters with the highest number of candidate TF interactions identified by eY1H, and for which binding sites were also detected in DAP-seq (Fig. 3). Shoot and root organs from these validated lines were collected separately to capture potential organ-specific regulation. qRT-PCR analyses revealed consistent significant differences in *PSYR* and *PSY* expression (Fig. 3), directly connecting TF-promoter interactions to transcriptional outputs.

Most mutants showed altered expression of *PSYR*/*PSY* target genes, with distinct patterns of activation and repression. MYB70 bound the promoters of both *PSYR1* and *PSYR2* and repressed their transcription, whereas MYB73 bound the *PSYR1* promoter but acted in an organ-specific manner, repressing transcription in shoots while activating it in roots. CRF10 bound the *PSYR3* promoter and activated transcription in both organs, while TGA5 and WRKY8 each activated *PSY1* transcription. In contrast, ABI5 consistently functioned as a repressor, binding both *PSY1* and *PSY4* promoters and reducing expression in shoots and roots. Finally, RAV2.11 bound the *PSY2* promoter and exerted opposite effects across organs, activating transcription in shoots while repressing it in roots (Fig. 3 and Data S4). These transcriptional outcomes are consistent with direct TF-mediated regulation, and the magnitude and organ specificity of expression changes paralleled the growth phenotypes of the corresponding knockout lines, supporting a model in which these TFs fine-tune PSY signaling through spatially resolved transcriptional control. Overall, these results show that organ-specific expression patterns of *PSYR* and *PSY* genes are supported by large-scale TF-promoter interaction data, and support a model in which combinations of transcription factors coordinate spatial PSY signaling, ultimately influencing growth and RSA phenotypes.

Precision promoter editing of *PSYR3* reshapes root growth

To test whether disruption of transcription factor binding sites could modulate gene expression and plant growth, we implemented a CRISPR/Cas9-based promoter editing strategy. Candidate motifs within *PSYR* and *PSY* promoters were targeted, focusing initially on the *PSYR3* promoter. A putative CRF10 binding motif ('CGGCGG') was identified in the *PSYR3* promoter using DAP-seq data and validated by eY1H. CRF10 is a member of the APETALA2 (AP2)/ETHYLENE RESPONSE FACTOR (ERF) transcription factor family, which regulates hormone signaling, stress responses, and development[29]. Although the *Arabidopsis* CRF family contains 12 members, CRF10 remains largely uncharacterized. In Col-0 plants, *CRF10* was expressed ubiquitously, with the highest expression in embryos (Fig. S4). In our screening (Fig. 2), *crf10* mutants exhibited longer primary roots and overall enhanced root system architecture (RSA), characterized by increased lateral root number and length as well as greater total root

length. Overexpression of *CRF10* in wild-type Col-0 caused growth inhibition, confirming that *CRF10* functions as a negative regulator of growth (Fig. S7). To directly test whether CRF10 binding influences *PSYR3* expression, we generated CRISPR-edited lines targeting the CRF10 motif in the *PSYR3* promoter. Two guide RNAs were designed to target both the primary TFBS and adjacent sequences (Fig. 4a). Sequencing of independent lines revealed two distinct alleles. R3pro_Var1 carries a 31 bp deletion immediately adjacent to the DAP-seq-validated CRF10 binding motif, leaving the consensus sequence intact, whereas R3pro_Var2 carries a 27 bp deletion that removes the motif entirely. T2 homozygous lines were used for phenotyping and expression assays.

Phenotypic analysis revealed that promoter-edited plants exhibited altered primary root length compared with wild type, with phenotypes comparable in magnitude to *psyr3-1* and *crf10* knockout mutants (Fig. 4c). Lateral root number remained unchanged (Fig. 4d), but total lateral root length per plant increased (Fig. 4e), resulting in increased total and average lateral root length relative to WT, *psyr3-1*, and *crf10* (Fig. 4f). Both edited alleles also displayed reduced *PSYR3* transcript abundance in the shoot and root relative to wild-type controls (Fig. 4g), with R3pro_Var1 showing reduced expression despite retaining the CRF10 consensus motif, suggesting that sequences adjacent to the motif also contribute to transcriptional regulation.

Discussion

Our work demonstrates the utility of network-guided promoter editing to fine-tune gene expression through genome editing of transcription factor binding sites. Phenotypic and expression changes in promoter-edited *PSYR3* lines confirm that disrupting predicted regulatory motifs can produce measurable biological outcomes. Notably, altered expression was observed not only when the CRF10 binding motif itself was deleted, but also when nearby promoter regions were perturbed, which may reflect the involvement of additional regulatory sites. These results indicate that promoter edits can influence transcriptional activity beyond direct motif removal, emphasizing the importance of local sequence context, motif spacing, DNA structure, and *cis*-regulatory modules in shaping transcriptional output. Even small alterations outside core transcription factor binding sites were sufficient to affect transcription, demonstrating the sensitivity of regulatory networks to local sequence changes. The observation that promoter edits produced phenotypes comparable to gene knockouts illustrates both the promise and complexity of this approach. While transcription factor binding site-level editing allows finer control than complete gene disruption, it also reveals buffering and redundancy inherent in plant regulatory networks. Divergence between *psyr3-1* and *crf10* knockout phenotypes suggests that CRF10 regulates additional downstream targets, while *PSYR3* is likely influenced by multiple transcription factors. These findings highlight that single-site promoter perturbations may only partially recapitulate gene knockout effects, reflecting the distributed nature of transcriptional control. Together, these results underscore the need to consider promoter architecture, motif spacing, and network connectivity when designing targeted edits, as subtle changes can have wide-ranging effects on transcriptional output.

Beyond mechanistic insights, network-guided promoter editing enables precise, context-aware trait modulation. By leveraging functional cis elements identified from regulatory networks, edits can be tailored for spatially precise regulation at the organ, tissue, or even cell level, in addition to being environment-responsive, thereby enhancing trait specificity while minimizing unintended systemic effects. This capability is particularly valuable for complex traits influenced by multiple environmental and developmental cues, where traditional knockout approaches may produce broad pleiotropic effects. Sequences adjacent to transcription factor binding sites contribute significantly to transcriptional output, as even minor alterations can perturb expression. These observations suggest that combinatorial editing of multiple sites within a gene, or across several targets of the same transcription factor, is likely necessary to overcome redundancy and achieve predictable phenotypic outcomes. Such combinatorial strategies can enhance control over quantitative traits and increase the robustness of phenotypic outcomes across different genetic backgrounds and environmental conditions. By integrating spatial- and condition-specific regulatory information, network-guided promoter editing enables rationally designed edits that tune gene expression in the desired context, providing nuanced control over activity. Altogether, these approaches move plant engineering beyond binary knockouts and toward tunable modulation, providing a framework for optimizing traits while preserving overall plant fitness.

Although tiling-deletion-based screens have enabled systematic functional interrogation of regulatory regions, they are labor-intensive, time-consuming, and often less predictive, particularly when applied across multiple genes. Moreover, because these strategies rely on scanning promoter regions through serial deletion or mutagenesis, they tend to reveal functional elements retrospectively rather than enabling targeted modulation. In contrast, our gene regulatory network-guided strategy enables precise selection of functional *cis*-regulatory elements, increasing specificity while reducing experimental complexity. This hypothesis-driven approach facilitates fine-tuning at the gene family level and is compatible with high-throughput, NGS-based genotyping, enabling accurate identification of edited genotypes. By narrowing the range of potential target sites, network-guided editing enhances both predictability and efficiency, laying the groundwork for downstream applications such as base editing or prime editing to precisely tune transcription factor binding sites. Although promoter insertions or swaps remain technically challenging, successful examples, such as the insertion of the *GOS2* promoter upstream of *ARGOS8* in maize to enhance expression and improve drought tolerance[30], demonstrate the potential for context-aware regulatory engineering and create opportunities for synthetic promoter applications by replacing native promoters.

Promoter editing in Arabidopsis remains largely unexplored, yet the species offers rich genomic and regulatory resources, including well-characterized gene regulatory networks, TFBS maps, and promoter motifs. Comparative analyses between Arabidopsis and crop species will be essential to translate these insights to agricultural contexts. While gene regulatory networks are extensively mapped in Arabidopsis, coverage in major crops remains limited. Systematic comparisons of TFBSs, promoter architectures, and regulatory modules can identify conserved elements, enabling rational design of network-guided promoter edits in crop species. Integrating comparative genomics with functional validation in crops will allow predictions from Arabidopsis to inform trait optimization

strategies, including stress resilience, yield improvement, and adaptation to fluctuating environmental conditions. By leveraging evolutionary conservation and incorporating species-specific regulatory data, network-guided editing can bridge the gap between model systems and practical agricultural applications, providing a roadmap for translational *cis*-regulatory engineering.

Future studies will explore how promoter edits impact local chromatin accessibility and higher-order regulatory architecture, as well as downstream physiological responses such as environmental stress adaptation and pathogen resistance. Integrating ATAC-seq or other chromatin profiling approaches in edited lines will provide deeper insight into the epigenomic consequences of TFBS-level perturbations and help refine predictive models of *cis*-regulatory engineering. Beyond chromatin accessibility, advanced chromatin conformation capture techniques, such as Hi-C, and super-resolution microscopy will enable mapping of long-range chromatin interactions and three-dimensional promoter-enhancer organization. These approaches will reveal how network-guided promoter edits influence not only local accessibility but also broader regulatory networks. Collaborative integration of epigenomic and imaging data will facilitate comprehensive models linking *cis*-regulatory perturbations to transcriptional and phenotypic outcomes. Extending these analyses across spatial and environmental conditions will further enhance the ability to design edits that achieve context-specific gene regulation while minimizing unintended effects. Additionally, expanding this strategy to include base editing, prime editing, and combinatorial promoter modifications will increase the precision and versatility of *cis*-regulatory engineering. Collectively, these approaches will accelerate the development of crops with optimized traits, improved stress resilience, and enhanced performance across diverse environments.

Methods

Promoter cloning for eY1H.

PSYR and *PSY* gene promoters previously tested in Ogawa-Ohnishi et al.[1] were cloned using the method described by Gaudinier et al.[22,31]. Promoters were amplified by PCR from *Arabidopsis thaliana* Col-0 genomic DNA using Phusion High-Fidelity DNA Polymerase (NEB). The amplified promoter fragments were first cloned into the pENTR 5'TOPO vector using the pENTR 5'TOPO kit (Invitrogen) and fully sequenced. Subsequently, promoters were recombined with the Gateway LR reaction into both pMW2 and pMW3[30] Gateway destination vectors (designed for yeast expression and containing respectively *HIS3* or *LacZ* reporter genes) using LR Clonase™ II (Invitrogen). The resulting constructs were sent to Azenta Life Sciences (South Plainfield, NJ, USA; formerly GeneWiz) for whole plasmid sequencing using the Plasmid-EZ nanopore-based sequencing method.

Enhanced Yeast One Hybrid (eY1H) Assay.

Assays were performed according to Gaudinier et al.[22,31]. *PSYR* and *PSY* promoter – pMW2/pMW3 reporter constructs were transformed into yeast strain YM4271. Resulting

yeast colonies were screened for autoactivation for both histidine biosynthesis and lacZ activity, and the construct presence within the yeast genome was confirmed by PCR-based genotyping. The resulting bait yeast strains were screened against a complete collection of 2000 Arabidopsis transcription factors[32] in a mating-based assay, and positive interactions were identified for both histidine and lacZ activity compared to a negative control pDESTAD-2μ. An interaction was recorded as successful if there was activation of either HIS or lacZ. The eY1H Yeast One-Hybrid screening was carried out by the Yeast One-Hybrid Services Core at the UC Davis Genome Center, at the University of California, Davis. The table with all the results can be found at https://github.com/jcyliao/Liao2025.

Network construction.

Networks were made using Cytoscape v.3.10.2[33]. All cytoscape network files can be found at https://github.com/jcyliao/Liao2025.

DAP-seq data comparison and mutant lines selection.

DAP-seq TF binding data generated by O'Malley et al.[21] were used to identify direct TF-promoter interactions. DAP-seq target genes (fraction of reads in peaks [FRiP] ≥ 5%) for 529 TFs were downloaded from the Plant Cistrome Database. TFs binding to each individual *PSYR*/*PSY* promoter were extracted from the DAP-seq data (Dataset S1). A Python script was then used to compare the TF lists for each promoter from eY1H and DAP-seq experiments, generating lists of overlapping TFs identified by both assays (Dataset S2).

From these comparisons, 40 overlapping TFs and ~20 TFs identified only in DAP-seq were selected based on the availability of loss-of-function mutants. Mutant lines previously used in published studies were prioritized (Table S2).

Expression analysis of *PSYR*/*PSY* genes and their regulatory TFs.

Expression patterns of *PSYR* and *PSY* genes, along with their selected potential regulatory transcription factors (TFs) identified from eY1H and DAP-seq, were analyzed using publicly available datasets. Bulk RNA-seq datasets were collected to examine gene expression across different tissues and developmental stages. Single-cell RNA-seq datasets, including root cell type-specific profiles from the Plant sc-Atlas database[26], were used to assess cell type-specific expression. Comparative analyses were performed to identify co-expression patterns and potential tissue- or cell type-specific regulatory relationships.

Plant materials and growth conditions.

All transgenic lines were generated in the *Arabidopsis thaliana* Col-0 accession, except for *abi5-1*, which was in the Ws-2 background. Loss-of-function TF mutants were obtained from the Arabidopsis Biological Resource Center (ABRC) at Ohio State University. All mutant lines, including those carrying T-DNA insertions, fast neutron-induced mutations, or EMS-induced mutations, were genotyped to confirm homozygosity. Quantitative RT-PCR (qRT-PCR) was performed to verify transcript-level alterations (Fig. S5 and Data S4). The primers used for genotyping and qRT-PCR, along with accession numbers and additional details on the analyzed mutant lines, are provided in Supplementary Table 2. Plants were grown under a 16-hour light/8-hour dark photoperiod for propagation.

Generation of TF overexpressing transgenic plants.

The coding sequences for each TF used in this study were obtained from the TF ENTR clone collection[32] and subsequently cloned into the N-GFP tag pGWB506 (Addgene #74848) destination vector using LR Clonase™ II (Invitrogen) for overexpression in plants. The resulting GFP-TF constructs, driven by the 35S promoter, were introduced into *Agrobacterium tumefaciens* strain GV3101 and used to transform *A. thaliana* (Col-0) via the floral dip method[34]. Transgenic lines were selected on ½ MS solid medium supplemented with 25 mg/L hygromycin. Transgene expression was assessed through GFP fluorescence microscopy, PCR, and qRT-PCR. T3 homozygous plants were used for subsequent phenotypic analyses. The primers used for genotyping and accession numbers, and additional details on the constructs, are provided in Supplementary Table 1.

Plant phenotype analysis of the TF mutants.

Homozygous TF loss-of-function mutants, TF overexpression T3 plants, and the wild-type (WT) controls seeds were sterilized with 25% (v/v) bleach for 20 min, followed by 5 washes with sterile Milli-Q water. Sterilized seeds were plated on ½ MS medium supplemented with 1% sucrose and 0.6% Gelzan, then stratified at 4°C for 2-3 days before being transferred to a growth chamber under long-day (LD) conditions (16 h light/8 h dark) with 50-60% humidity at 22°C. Mutant lines and wild-type controls were arranged in a randomized block design within the growth chamber. Plate images were scanned at 10 days post-germination (10 dpg) using an Epson Expression 12000XL scanner at 300 dpi resolution. Root traits were measured from the scanned images, with at least 20 plants per genotype included in each experimental replicate. For root trait measurements, RootNav 1.0[35] was used for image analysis and data extraction. Traits measured included primary root length (PRL), lateral root number (LR) and lateral root length (LRL). Composite traits were analyzed, including total root length (TRL = PRL + LRL), average lateral root length (ALRL = LRL/LR), lateral root density (LRD = LR/PRL), and the percentage of LRL contributing to TRL (LRL/TRL). Variation across these mutants relative to WT was assessed using one-way ANOVA for all RSA traits. Statistical analyses were performed in Python, with significance determined by Tukey's HSD test.

424 **RNA extraction and quantitative PCR.**

425 The whole root and shoot parts of 10-day-old seedlings were collected separately. For
426 one shoot sample, shoots from 10 seedlings grown on the same plate were pooled
427 together. For one root sample, roots from 30 seedlings grown on the same plate were
428 pooled together. Three independent replicates per genotype were collected. Total RNA
429 was extracted using TRIzol reagent (Invitrogen) for TF mutant screening experiments
430 and using the RNeasy Plant Mini Kit (QIAGEN) for promoter-edited line experiments,
431 following the manufacturer's instructions. Genomic DNA contamination was removed by
432 RNase-free DNase treatment during RNA extraction, according to the manufacturer's
433 protocols. First-strand cDNA was synthesized using the SuperScript™ III First-Strand
434 Synthesis System for RT-PCR (Invitrogen) following the manufacturer's instructions.
435 Quantitative real-time PCR (qRT-PCR) was performed using iTaq™ Universal SYBR
436 Green Supermix (Bio-Rad) on a Bio-Rad CFX96 Real-Time System coupled with a
437 C1000 Thermal Cycler (Bio-Rad) under the following conditions: initial denaturation at
438 95°C for 30 s, followed by 39 cycles of PCR (denaturation at 95°C for 5 s, annealing at
439 60°C for 30 s, and extension at 72°C for 20 s). Relative gene expression was
440 determined using the $2^{-\Delta\Delta CT}$ method, with ACTIN2 as the endogenous control. The
441 primers used for qRT-PCR are provided in Supplementary Table 1.
442

443 **Generation of CRISPR/Cas9 promoter editing constructs and plant screening**

444 To precisely modulate transcription factor (TF) binding at the *PSY* and *PSYR* gene
445 promoters, we employed a targeted promoter editing approach using CRISPR/Cas9. This
446 strategy enables deletion or mutation of specific TF binding sites (TFBSs) to disrupt
447 repressive *cis*-regulatory elements and fine-tune gene expression. Promoter regions
448 containing characterized TFBSs were selected based on TF-promoter interaction
449 mapping and mutant phenotypes. Guide RNAs (gRNAs) were designed to flank these
450 sites, and corresponding CRISPR/Cas9 constructs were generated using standard
451 cloning protocols.

452 For the generation of pJL-AtU6.26-gPSYR3-S1S2 entry clone, an EcoRI–AtU6-26
453 promoter-partial pQZ435–BsaI gBlock was synthesized via the IDT gBlock service.
454 gRNAs were designed using CHOPCHOP[36], and PTG assembly into pQZ435, with the
455 OsU3 promoter removed, was performed following Xie et al.[37] with minor modifications.
456 The entry clone was transferred into the pRU294 destination vector via Gateway LR
457 recombination, following the manufacturer's instructions, and the resulting construct was
458 transformed into *Agrobacterium tumefaciens* GV3101 for plant transformation. Constructs
459 were transformed into *Arabidopsis thaliana* via Agrobacterium-mediated floral dipping.
460 Rapid screening of Cas9-containing and Cas9-free lines in both T1 and T2 generations
461 was conducted using a seed coat fluorescence marker[38]. Transgenic plants were
462 confirmed by PCR and Sanger sequencing to confirm precise edits disrupting TFBSs.
463 Successfully edited lines were propagated for subsequent phenotypic and gene
464 expression analyses.

465

466 **Figure preparation and statistical analysis**

Python was used for statistical analyses and to generate plots. Figures were assembled in Adobe Illustrator. Some illustrations in the workflow (Fig. 2a) were created using BioRender.

Data availability

All supplementary datasets, Cytoscape files, and Python code are available at https://github.com/jcyliao/Liao2025.

Acknowledgements

We thank Bhanu Upadhyayula, Kai Deshpande, and Maya Ziebarth for assistance with organizing genetic materials and performing genotyping experiments. We are also grateful to Valley Stewart for guidance and mentoring, and to Qiong Zhang for providing the pQZ435 vector and the modified PTG cloning protocol. This work was supported by the Chan Zuckerberg Initiative and NIH MIRA grant #R35 GM148173 to P.C.R.

Author contributions

J.C.-Y.L. conceived the project, designed the experiments, and conducted most of the experiments and all data analysis. A.B. and the Yeast One-Hybrid (Y1H) Services Core conducted all eY1H screenings. J.C.-Y.L. and A.J.L. prepared samples for the gene expression assays. A.J.L. performed most of the root phenotyping raw data acquisition and, together with Y.S., carried out qRT-PCR measurements. Both A.J.L. and Y.S. participated in mutant screening. P.C.R. supervised the work and provided funding and resources. J.C.-Y.L. wrote and revised the manuscript with input from S.M.B. and edits from P.C.R.

References

1. Ogawa-Ohnishi, M. *et al*. Peptide ligand-mediated trade-off between plant growth and stress response. *Science* **378**, 175–180 (2022).

2. Wang, Y., Chen, W., Ou, Y., Zhu, Y. & Li, J. Arabidopsis ROOT ELONGATION RECEPTOR KINASES negatively regulate root growth putatively via altering cell wall remodeling gene expression. *J Integr Plant Biol* **64**, 1502–1513 (2022).

3. Ercoli, M. F., Shigenaga, A. M., Araujo, A. T. de, Jain, R. & Ronald, P. C. Tyrosine-sulfated peptide hormone induces flavonol biosynthesis to control elongation and differentiation in Arabidopsis primary root. 2024.02.02.578681 Preprint at https://doi.org/10.1101/2024.02.02.578681 (2024).

502 4. Yimer, H. Z. *et al.* Root-knot nematodes produce functional mimics of tyrosine-
503 sulfated plant peptides. *Proceedings of the National Academy of Sciences* **120**,
504 e2304612120 (2023).

505 5. Ercoli, M. F. *et al.* Plant immunity: Rice XA21-mediated resistance to bacterial
506 infection. *Proc. Natl. Acad. Sci. U. S. A.* **119**, (2022).

507 6. Li, Q., Sapkota, M. & van der Knaap, E. Perspectives of CRISPR/Cas-mediated cis-
508 engineering in horticulture: unlocking the neglected potential for crop improvement.
509 *Hortic Res* **7**, 1–11 (2020).

510 7. Rodríguez-Leal, D., Lemmon, Z. H., Man, J., Bartlett, M. E. & Lippman, Z. B.
511 Engineering Quantitative Trait Variation for Crop Improvement by Genome Editing.
512 *Cell* **171**, 470-480.e8 (2017).

513 8. Liu, L. *et al.* Enhancing grain-yield-related traits by CRISPR–Cas9 promoter editing
514 of maize CLE genes. *Nat. Plants* **7**, 287–294 (2021).

515 9. Song, X. *et al.* Targeting a gene regulatory element enhances rice grain yield by
516 decoupling panicle number and size. *Nat Biotechnol* **40**, 1403–1411 (2022).

517 10. Duan, Y.-B. *et al.* Identification of a regulatory element responsible for salt
518 induction of rice OsRAV2 through ex situ and in situ promoter analysis. *Plant Mol*
519 *Biol* **90**, 49–62 (2016).

520 11. Xu, Z. *et al.* Engineering Broad-Spectrum Bacterial Blight Resistance by
521 Simultaneously Disrupting Variable TALE-Binding Elements of Multiple
522 Susceptibility Genes in Rice. *Molecular Plant* **12**, 1434–1446 (2019).

523 12. Li, C. *et al.* A new rice breeding method: CRISPR/Cas9 system editing of the Xa13
524 promoter to cultivate transgene-free bacterial blight-resistant rice. *Plant*
525 *Biotechnology Journal* **18**, 313–315 (2020).

526 13. Oliva, R. *et al.* Broad-spectrum resistance to bacterial blight in rice using genome
527 editing. *Nat Biotechnol* **37**, 1344–1350 (2019).

528 14. Holme, I. B. *et al.* Evaluation of the mature grain phytase candidate HvPAPhy_a
529 gene in barley (Hordeum vulgare L.) using CRISPR/Cas9 and TALENs. *Plant Mol Biol*
530 **95**, 111–121 (2017).

531 15. Jia, H., Orbović, V. & Wang, N. CRISPR-LbCas12a-mediated modification of citrus.
532 *Plant Biotechnology Journal* **17**, 1928–1937 (2019).

533 16. Jia, H., Orbovic, V., Jones, J. B. & Wang, N. Modification of the PthA4 effector binding
534 elements in Type I CsLOB1 promoter using Cas9/sgRNA to produce transgenic

535 Duncan grapefruit alleviating XccΔpthA4:dCsLOB1.3 infection. *Plant Biotechnology*
536 *Journal* **14**, 1291–1301 (2016).

537 17. Peng, A. *et al.* Engineering canker-resistant plants through CRISPR/Cas9-targeted
538 editing of the susceptibility gene CsLOB1 promoter in citrus. *Plant Biotechnol. J.* **15**,
539 1509–1519 (2017).

540 18. Li, T. *et al.* Domestication of wild tomato is accelerated by genome editing. *Nat*
541 *Biotechnol* **36**, 1160–1163 (2018).

542 19. Li, X. *et al.* Programmable base editing of mutated TERT promoter inhibits brain
543 tumour growth. *Nat Cell Biol* **22**, 282–288 (2020).

544 20. Tang, M. *et al.* A genome-scale TF–DNA interaction network of transcriptional
545 regulation of Arabidopsis primary and specialized metabolism. *Molecular Systems*
546 *Biology* **17**, e10625 (2021).

547 21. O'Malley, R. C. *et al.* Cistrome and Epicistrome Features Shape the Regulatory DNA
548 Landscape. *Cell* **165**, 1280–1292 (2016).

549 22. Gaudinier, A. *et al.* Enhanced Y1H assays for Arabidopsis. *Nat Methods* **8**, 1053–
550 1055 (2011).

551 23. Gaudinier, A. *et al.* Transcriptional regulation of nitrogen-associated metabolism
552 and growth. *Nature* **563**, 259–264 (2018).

553 24. Sparks, E. E. *et al.* Establishment of Expression in the SHORTROOT-SCARECROW
554 Transcriptional Cascade through Opposing Activities of Both Activators and
555 Repressors. *Developmental Cell* **39**, 585–596 (2016).

556 25. Zhang, H. *et al.* A Comprehensive Online Database for Exploring ~20,000 Public
557 Arabidopsis RNA-Seq Libraries. *Molecular Plant* **13**, 1231–1233 (2020).

558 26. Wendrich, J. R. *et al.* Vascular transcription factors guide plant epidermal
559 responses to limiting phosphate conditions. *Science* **370**, eaay4970 (2020).

560 27. Amano, Y., Tsubouchi, H., Shinohara, H., Ogawa, M. & Matsubayashi, Y. Tyrosine-
561 sulfated glycopeptide involved in cellular proliferation and expansion in
562 Arabidopsis. *Proc Natl Acad Sci U S A* **104**, 18333–18338 (2007).

563 28. Wan, J. *et al.* MYB70 modulates seed germination and root system development in
564 Arabidopsis. *iScience* **24**, 103228 (2021).

565 29. Rashotte, A. M. *et al.* A subset of Arabidopsis AP2 transcription factors mediates
566 cytokinin responses in concert with a two-component pathway. *Proceedings of the*
567 *National Academy of Sciences* **103**, 11081–11085 (2006).

30. Shi, J. *et al.* ARGOS8 variants generated by CRISPR-Cas9 improve maize grain yield under field drought stress conditions. *Plant Biotechnology Journal* **15**, 207–216 (2017).

31. Gaudinier, A., Tang, M., Bågman, A.-M. & Brady, S. M. Identification of Protein–DNA Interactions Using Enhanced Yeast One-Hybrid Assays and a Semiautomated Approach. in *Plant Genomics: Methods and Protocols* (ed. Busch, W.) 187–215 (Springer, New York, NY, 2017). doi:10.1007/978-1-4939-7003-2_13.

32. Pruneda-Paz, J. L. *et al.* A Genome-Scale Resource for the Functional Characterization of Arabidopsis Transcription Factors. *Cell Reports* **8**, 622–632 (2014).

33. Shannon, P. *et al.* Cytoscape: A Software Environment for Integrated Models of Biomolecular Interaction Networks. *Genome Res.* **13**, 2498–2504 (2003).

34. Clough, S. J. & Bent, A. F. Floral dip: a simplified method for Agrobacterium-mediated transformation of Arabidopsis thaliana. *Plant J.* **16**, 735–43 (1998).

35. Pound, M. P. *et al.* RootNav: Navigating Images of Complex Root Architectures. *Plant Physiol* **162**, 1802–1814 (2013).

36. Labun, K. *et al.* CHOPCHOP v3: expanding the CRISPR web toolbox beyond genome editing. *Nucleic Acids Research* **47**, W171–W174 (2019).

37. Xie, K., Minkenberg, B. & Yang, Y. Boosting CRISPR/Cas9 multiplex editing capability with the endogenous tRNA-processing system. *Proceedings of the National Academy of Sciences* **112**, 3570–3575 (2015).

38. Ursache, R., Fujita, S., Dénervaud Tendon, V. & Geldner, N. Combined fluorescent seed selection and multiplex CRISPR/Cas9 assembly for fast generation of multiple Arabidopsis mutants. *Plant Methods* **17**, 111 (2021).

Figures

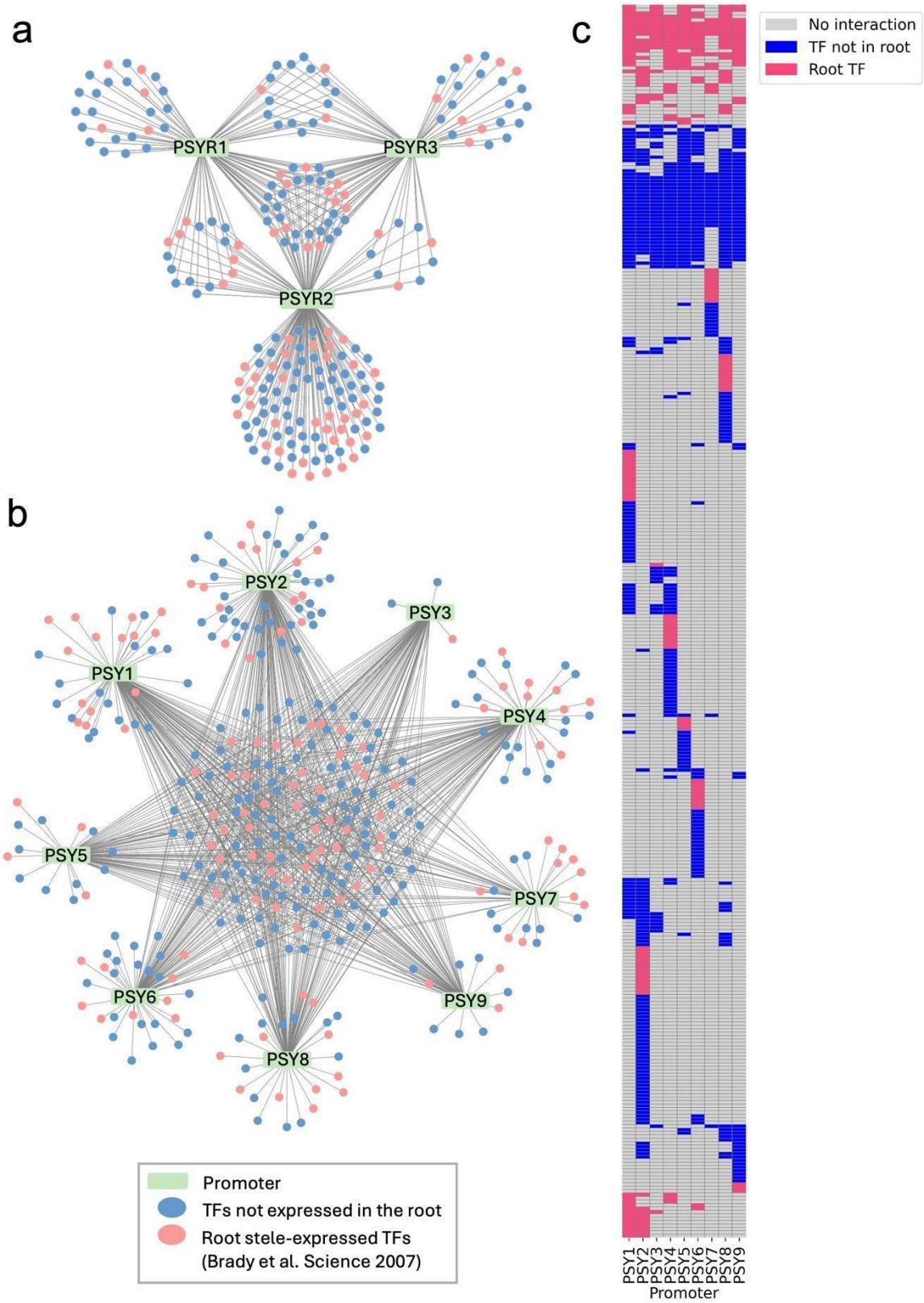

596

597 **Fig. 1. TF-*PSYR*/*PSY* promoter interaction network.**

598 **a.** TF-promoter interactions involved in PSY perception, identified by eY1H (*PSYR1-*
599 *PSYR3*, 3 promoters).
600 **b.** TF-promoter interactions involved in PSY peptide transcription, identified by eY1H
601 (*PSY1-PSY9*, 9 promoters). Rectangles represent promoters; small circles represent
602 TFs. Pink circles indicate root-expressed TFs (Brady et al., 2007), and blue circles
603 indicate TFs outside the root stele-expressed set.
604 **c.** Heatmap of TF-promoter interactions for PSY peptide transcription identified by
605 eY1H, with shared TFs clustered. Coloring follows panel b: pink = root-expressed TFs
606 (Brady et al., 2007), blue = TFs outside the root stele-expressed set.

607

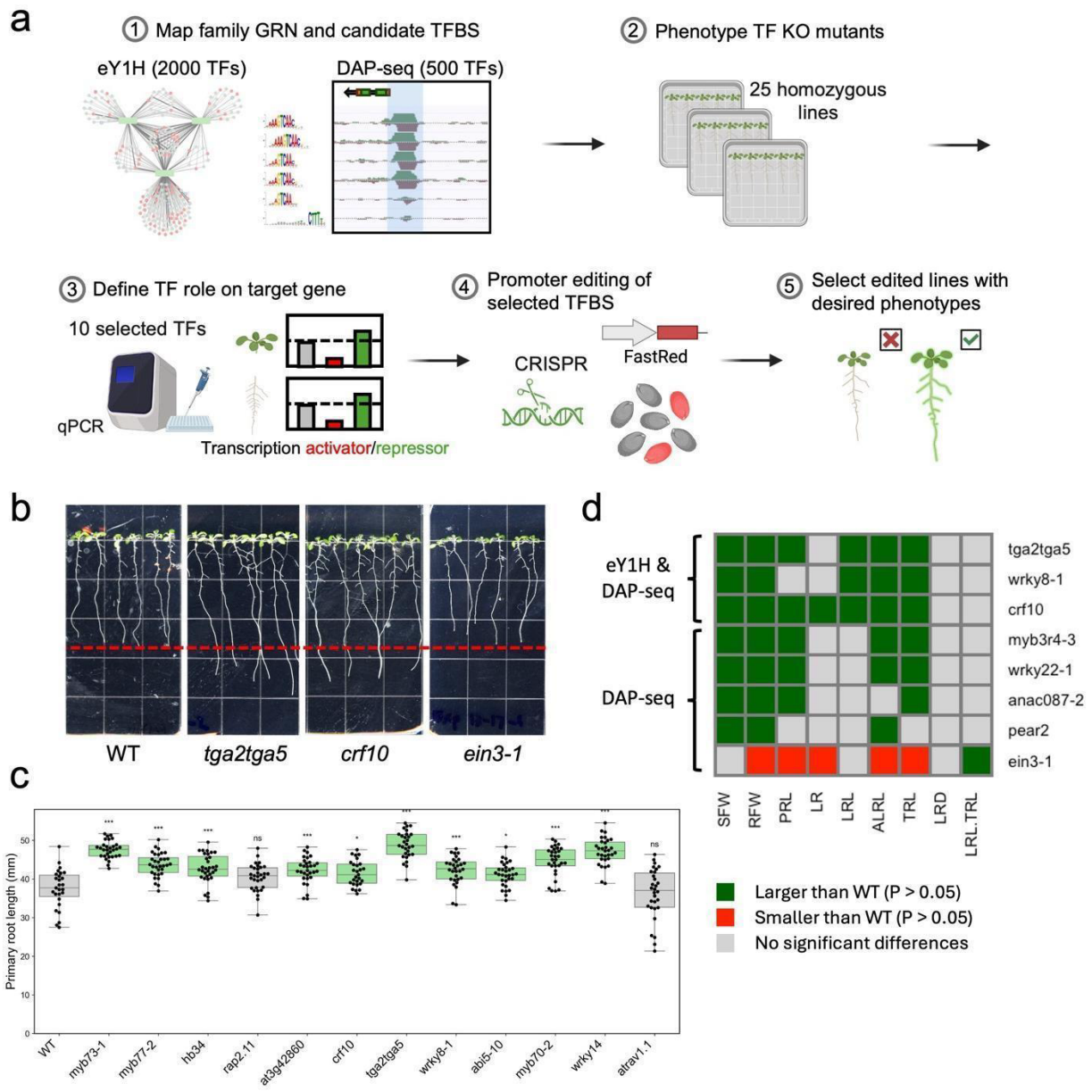

Fig. 2. Network-guided TFBS editing for precise promoter modification.
a. Schematic of the screening and editing workflow applied to *PSYR*/*PSY* promoters.
b. Representative 10-day-old TF knockout seedlings identified based on validated TF-promoter interactions. WT, Col-0.
c. Primary root length of 12 TF knockout mutants at 10 days old. Green indicates a statistically significant increase relative to WT, and grey indicates not significantly different ($P < 0.05$, one-way ANOVA; exact n and P values are in Supplementary Data 3).
d. Heatmap showing phenotypes associated with TF knockout alleles. Selected mutant alleles, identified from both eY1H and DAP-seq or from DAP-seq only, are listed in

619 rows, and measured traits are shown in columns. Statistically significant differences
620 relative to WT are indicated by colored cells ($P < 0.05$, one-way ANOVA; exact n and P
621 values are in Supplementary Data 3). From left to right, traits include shoot fresh weight
622 (SFW, g per 10 seedlings), root fresh weight (RFW, g per 10 seedlings), primary root
623 length (PRL, mm), number of lateral roots (LR), total lateral root length (LRL, mm), total
624 root length (TRL, PRL + LRL, mm), average lateral root length (ALRL, LRL/LR, mm),
625 lateral root density (LRD, LR/PRL), and proportion of total root length contributed by
626 lateral roots (LRL/TRL). Root traits were measured from 10-day-old seedlings. Green
627 indicates a statistically significant increase relative to WT, red indicates a statistically
628 significant decrease, and grey indicates not significantly different from WT ($P < 0.05$,
629 one-way ANOVA).

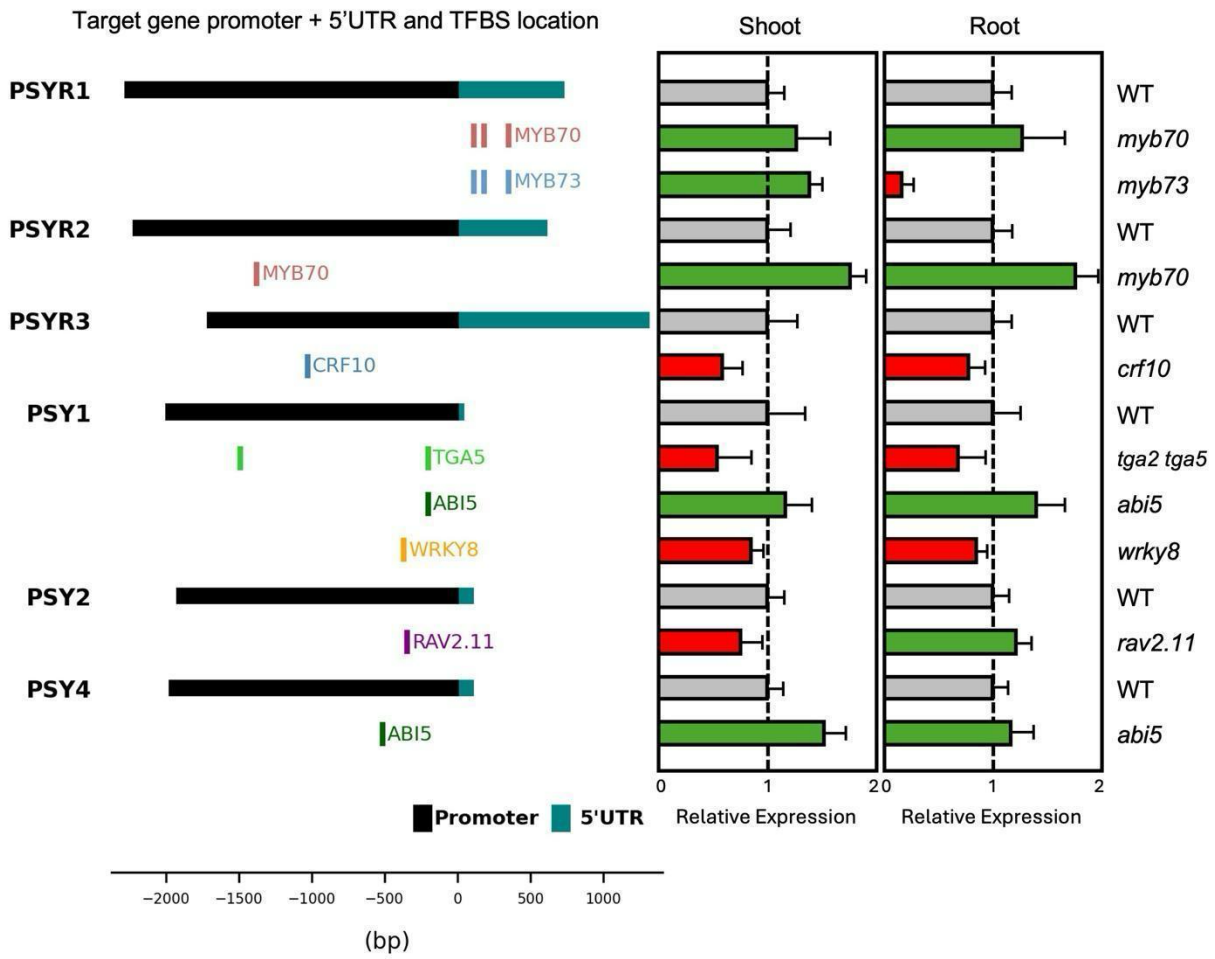

Fig. 3. Organ-specific transcriptional changes in TF knockout mutants.

Expression of targeted *PSYR*/*PSY* genes in seedling shoots and roots of 10-day-old TF knockout seedlings. Left, schematic of target *PSYR*/*PSY* promoters and 5'UTR showing the locations of transcription factor binding sites (TFBS) validated via DAP-seq. Right, relative expression of target *PSYR*/*PSY* genes in TF knockout seedlings. For each biological replicate, 10 shoots or 20 roots were pooled. Gene expression was measured by qRT-PCR, with WT normalized to 1 (grey bars). Expression levels significantly increased or decreased in the TF knockout relative to WT are indicated in green (TF is a transcriptional repressor) or red (TF is a transcriptional activator), respectively. Values represent mean ± SD (n = 3 biological replicates); exact *P* values are reported in Supplementary Data 4.

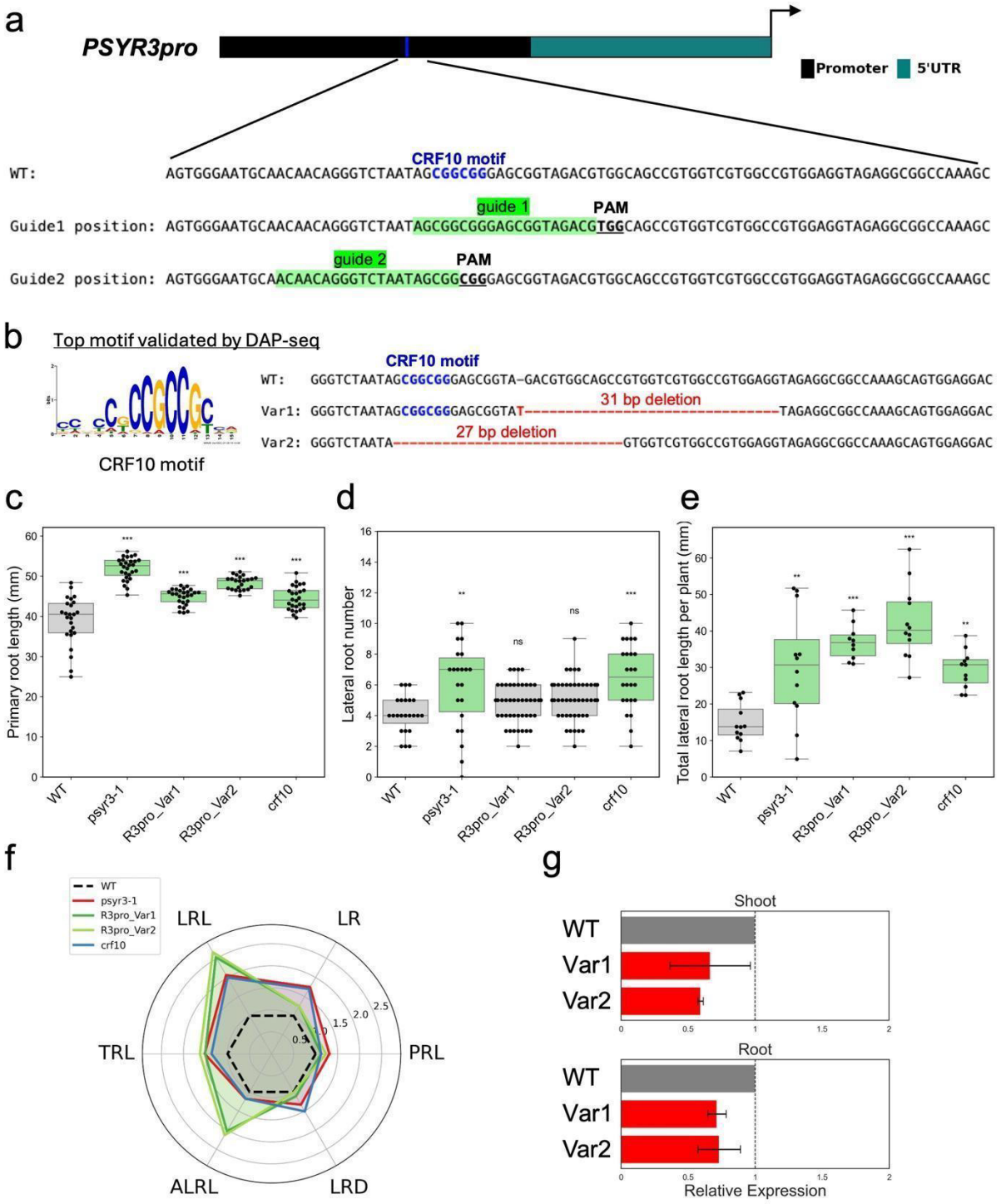

644

645 **Fig. 4. CRF10 motif editing in the *PSYR3* promoter boosts root growth.**

646 **a.** Schematic of the *PSYR3* promoter showing the CRF10 motif targeted for deletion.
647 **b.** DNA sequence comparison of two promoter-edited variants (Var1 and Var2) relative

648 to WT. Deleted CRF10 motifs are highlighted in red; dashes indicate deleted
649 nucleotides.
650 **c-f.** Root traits measured in 10-day-old seedlings.
651 **c.** Primary root length of WT, *psyr3-1*, *crf10*, and promoter-edited plants. Boxplots show
652 median, interquartile range, and full range.
653 **d.** Number of visible lateral roots per genotype.
654 **e.** Total lateral root length per genotype.
655 **f.** Radar plot comparing root traits across genotypes: PRL, primary root length (mm);
656 LR, number of lateral roots; LRL, total lateral root length (mm); ALRL, average lateral
657 root length (LRL/LR, mm); TRL, total root length (PRL + LRL, mm); LRD, lateral root
658 density (LR/PRL).
659 **g.** *PSYR3* expression in shoot and root organs of 10-day-old promoter-edited seedlings.
660 Values represent mean ± SD (n = 3 biological replicates); exact *P* values are reported in
661 Supplementary Data 4.
662

663

664 **Supplemental Materials**

665 All supplemental materials referenced in the text will be provided in the final published
666 version. All main findings are fully presented in the figures included in this manuscript.

667

668 **Supplementary Figures**

669

670 **Supplementary Fig. 1. Overlap of eY1H and DAP-seq interactions.**
671 Venn diagram showing TFs identified by either eY1H or DAP-seq for three *PSYR*
672 promoters and nine *PSY* promoters. Yellow circle indicates TFs identified by eY1H, and
673 blue circle indicates TFs identified by DAP-seq.

674 **Supplementary Fig. 2. *PSYR*/*PSY* expression at the whole plant level.**
675 Data were extracted from the public available bulk RNA-seq database.

676 **Supplementary Fig. 3. *PSYR*/*PSY* expression at the single-cell level in roots.**
677 Data were extracted from the Plant sc-Atlas database.

678 **Supplementary Fig. 4. Expression patterns of candidate TFs identified by both**
679 **eY1H and DAP-seq.**
680 Data were extracted from the public available bulk RNA-seq database.

681 **Supplementary Fig. 5. Confirmation of selected TF knockouts.**
682 qRT-PCR analysis of selected TF expression in TF knockout (KO) mutants. Gene

683 expression was measured by qRT-PCR and normalized to wild-type (WT = 1, grey
684 bars). Expression levels showing a significant decrease are indicated in red. Values
685 represent mean ± SD (n = 3 biological replicates); exact *P* values are reported in
686 Supplementary Data 4.

687 **Supplementary Fig. 6. Comparison of primary root length in selected Arabidopsis**
688 **mutant alleles of transcription factors identified by DAP-seq.**
689 Primary root length of 10 TF KO mutants at 10 days old. Exact *P* values are reported in
690 Supplementary Data 3.

691 **Supplementary Fig. 7. CRF10 acts as a negative regulator of plant growth.**
692 Overexpression of CRF10 causes an extreme dwarf phenotype. Forty-day-old adult
693 plants are shown. Scale bar = 1 cm.
694

695 **Supplementary Datasets**

696

697 **Supplementary Dataset 1.** List of eY1H results.

698 **Supplementary Dataset 2.** Overlap of eY1H and DAP-seq interactions.

699 **Supplementary Dataset 3.** RSA (root system architecture) phenotyping data.

700 **Supplementary Dataset 4.** qRT-PCR gene expression data.

701

702 **Supplementary Tables**

703

704 **Supplementary Table 1**. Genotyping, qRT-PCR, and cloning primers.

705 **Supplementary Table 2**. Summary of mutants, transgenic plants, and promoter-edited
706 plants.

707